Active Seismic Imaging of the Doty and Fall River Faults, Washington State: Excerpts from Geologic and Geophysical Assessment of Tectonic Uplift and Fault Activity in the Doty and Willapa Hills, Southwest Washington: Final Report

Experiment Name: Chehalis Basin Project Shallow Seismic Imaging
Nickname: CBP

Assembled by Megan Anderson[1], Travis West[1], Todd Lau[1], and Steve Bernsen[2]

1. Washington Geological Survey, Department of Natural Resources, 1111 Washington St., SE, MS 47007, Olympia, WA 98504
2. University of Maine, School of Earth and Climate Sciences, 5790 Bryand Global Sciences Center, Orono, ME, 04469

PURPOSE AND GUIDING RESEARCH QUESTIONS

Our goals were to determine if topographic features identified in the field and near-surface offsets from combined potential-field and geological cross-section modeling could be confirmed as fault related, and whether faults interpreted in this project have young deformation. As part of this goal, we tried to understand the location and orientation of fault planes and whether they deform Quaternary sediment, indicating recent activity. We employed a number of geophysical surveys for these investigations, including shallow-seismic reflection, direct-current resistivity, also called electrical resistivity tomography (ERT), and ground-penetrating radar (GPR). Using multiple geophysical methods provides insight into many different properties of the subsurface, thus narrowing the possible explanations of the subsurface geology and allowing for more-confident interpretation. Though we investigated 7 sites, only 2 included active seismic data collection & analysis (SG-6 and SG-7 in Figure 6-1). Further details about the data interpretation and combination with other constraints is in Steely and others (2021).

Overview of Method

Each geologic layer in the subsurface has its own acoustic impedance characteristics that relate to density and propagation velocity (Veeken and Van Moerkerken, 2013). Seismic reflection data can contribute to sediment thickness determination via impedance contrast between sedimentary layers and can profile abrupt changes in sedimentary package depth because seismic waves are sensitive to abrupt changes in density and seismic velocity (Telford and others 1990). Reflective interfaces are usually related to sedimentary bedding planes, unconformities and (or) porefill characteristics (Veeken and Van Moerkerken, 2013). Fault surfaces are generally not reflective and must be inferred by imaged offsets of lithologic packages (Telford and others, 1990).

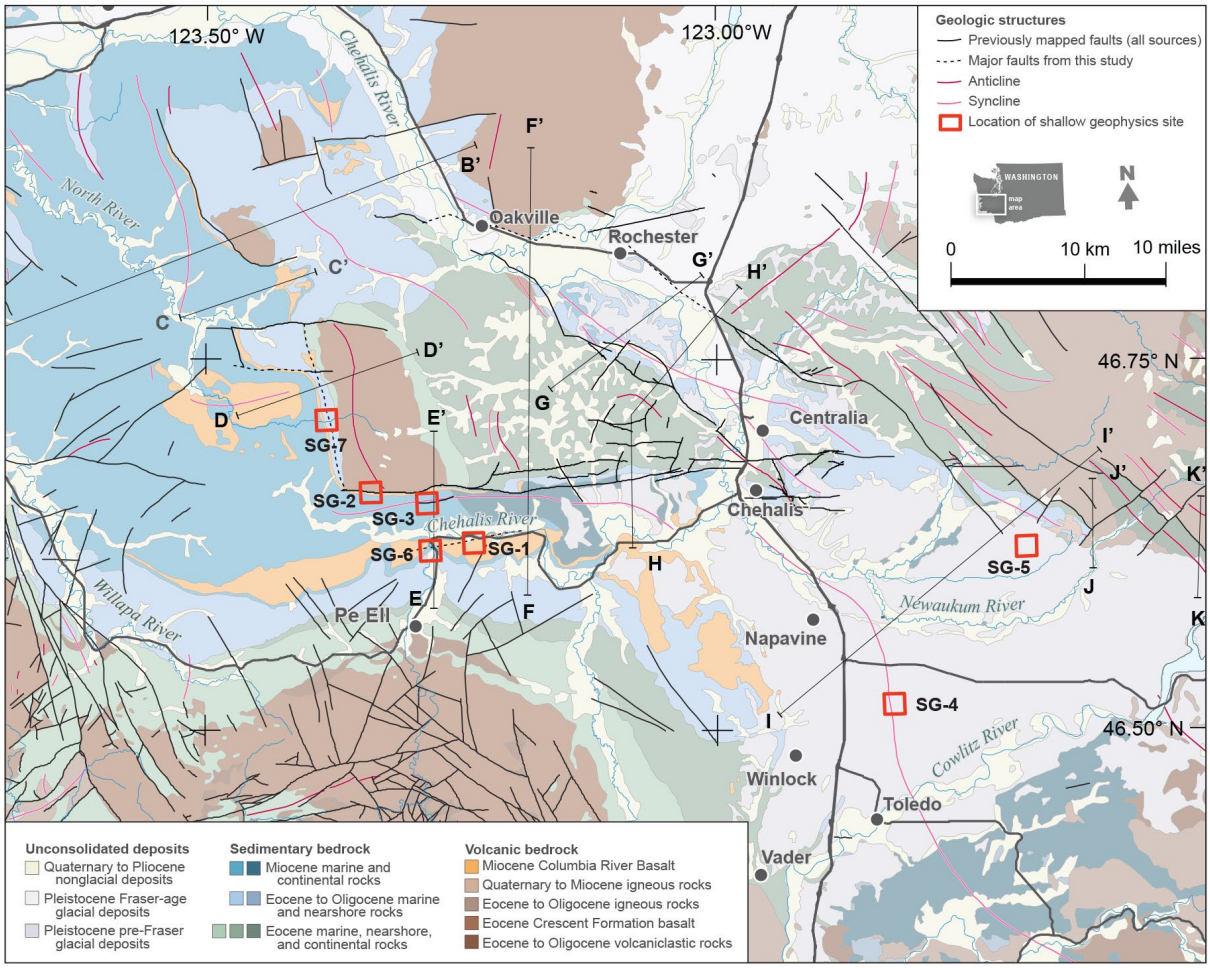

Figure 6-1. Location map with regional geology and shallow geophysical sites. Profiles B through K are geologic and geophysical cross sections discussed in Section 4. Geology is modified from Schasse (1987), Logan (1987, 2003a,b), Schuster and others (2016), Phillips (1987), Walsh (1987).

Site Selection

SG-6 (PE ELL GAP)

We were able to trace a lidar lineament described at site SG-1 west-southwest to site SG-6 where Quaternary alluvium along the modern Chehalis River provides an opportunity to examine the subsurface for young deformation (Figure 6-12). In addition, this location is where we interpret the Rainbow Falls fault in model E–E' (Figure 6-1) as projecting to the surface.

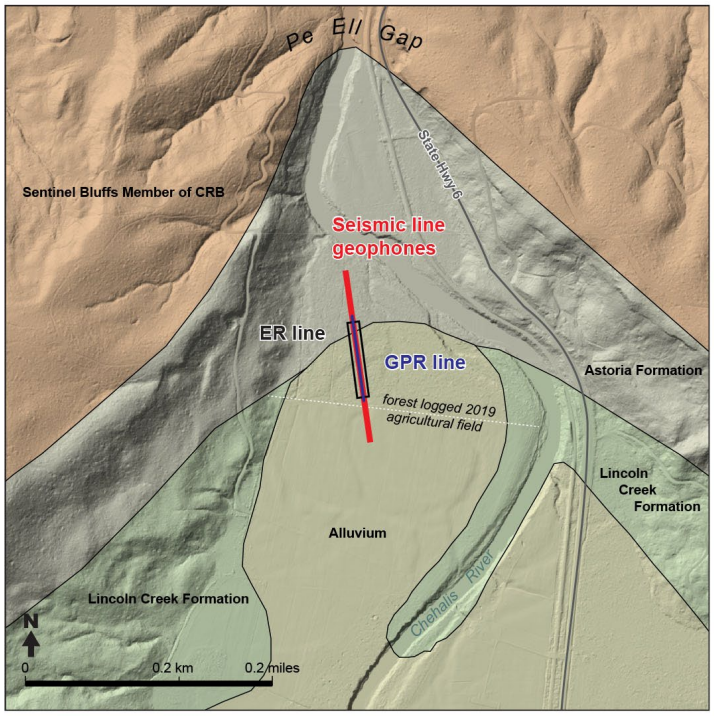

Figure 6-12 (left). Location map for site SG-6 showing electrode locations, GPR lines, geophone locations, and the boundary between recently logged forest (on the north) and an agricultural field (on the south). Geologic units are from Logan (1987).

SG-7 (FALL RIVER)

Potential-field modeling and geologic cross-section development supported our choice of site SG-7. The east-dipping reverse Fall River fault projects to the surface in this area within the Eocene to Oligocene Lincoln Creek Formation. To the east, uplifted and gently folded Eocene Crescent Formation is mapped within the Doty Hills and the Lincoln Creek uplift, and to the west lies steeply dipping (~70°) Miocene Sentinel Bluffs Member of the CRB which forms a prominent north–south trending ridge (Figure 6-16). At site SG-7, the projected fault is concealed by Quaternary alluvium of the Fall River. The seismic survey and the ER profile are collocated and centered on the projection of this fault as interpreted from the potential-field modeling.

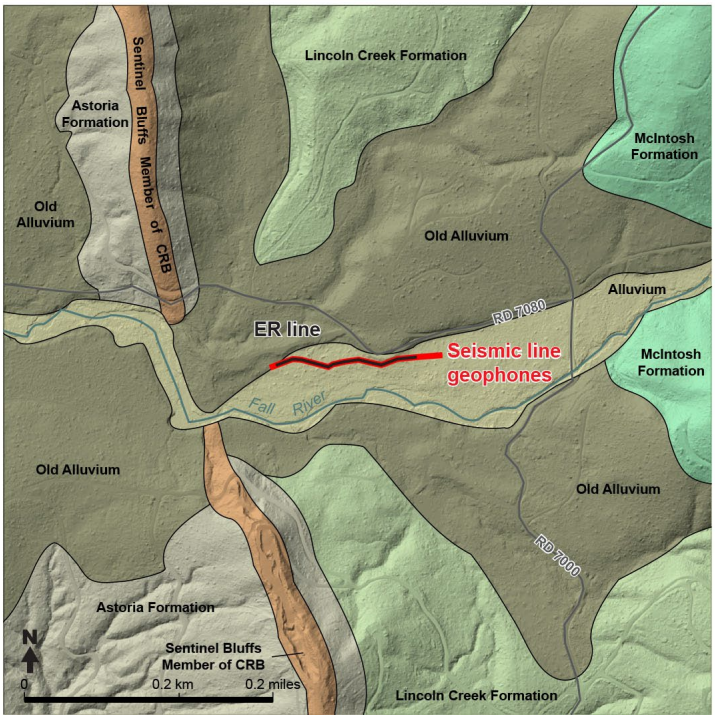

Figure 6-16 (left). Location map for site SG-7 showing electrode locations and geophone locations. Geology is modified from Logan (1987).

Field Methods

During June, 2020 a team from the Washington Geological Survey deployed two linear geophone arrays (spreads) to collect active seismic data for refraction and reflection analysis with the aim to characterize hypothesized faulting in the area. Each spread consisted of 192 channels with 2 m take-outs (geophone spacing) for a total spread length (aperture) of 382 m. The seismic lines maximized the 2-D subsurface coverage over the investigation area to image possible subsurface faulting. Moreover, for each spread, the orientation, take out, and aperture length maximized lateral resolution with a depth sampling down to 100 m.

Data collection followed field preparation, which included: vegetation removal, digging source pilot holes, equipment staging, and pre-deployment surveying. Each channel comprised a single 10-Hz vertical geophone, and eight 24-channel Geode digital seismographs recorded the data. Geodes were configured and synchronized into a single wired spread of 192 channels. Shot points were generally taken every 6 m in between geophones (every third half station), although the spacing varied some due to site conditions. Our spacing results in a maximum fold of 32 for both lines. Off-end shot points were also taken at 20 m and 40 m to maximize depth sampling for the refraction analysis. A Betsy SeisGun (BFG-500; Castillo Geophysical, Ltd.) using electronically fired 12-gauge blanks was the source for active data collection. Each Betsy shot was fired in a 0.2-m-diameter hole augured to a depth of approximately 0.75 m, backfilled with spoils, and doused with water and weighted for maximum coupling with the subsurface. At each shot point, one Betsy SeisGun "shot" was performed with trigger times provided via a hammer switch. Geometrics Seismodule Controller Software collected individual shot-gathers with a 0.25-ms sampling rate for 6.04-sec records and a high-cut (500 Hz) filter. Data at both sites were collected with the same parameters. Post-processed data from a Javad Triumph-2 GPS antenna provided geophone and shot point locations of each spread (Figures 6-13 and 6-17).

Results

Short descriptions of our results below illustrate the utility of the dataset. For details regarding tomographic and reflection seismic processing used to create these images, please refer to the original report (Steely and others, 2021).

Both 2-D P-wave refraction velocity models (Figures C-2 and C-3) extend past the geophone spread (between geophones 1 and 192) on either end to the farthest off-end shots for a total lateral extent of 460 m, and both models sample down to approximately 180 m depth. Inverted models converge to a reasonable root-mean-square uncertainty of 0.705 and 0.719 ms for the Fall River and Pe Ell lines respectively, depicting good overall sampling with overlapping ray paths down to 180 m depth in the model space between the geophones. However, outside the spread, both models are not adequately sampled and velocities are poorly constrained. It is important to keep in mind that during the process of iterating to a solution every cell in the model space is sampled at least once. Therefore, when looking at the ray path diagram through the final model, all areas of the model were at some point evaluated during the tomographic inversion.

Both Pe Ell (Figure C-2) and Rall River (Figure C-3) show similar trends in their respective final Vp models, depicting smooth velocity structure with strong lateral variations in the upper 60 m overlying mostly increasing velocity down to 180 m depth. For both models, the upper 6 m is mostly laterally continuous, with Vp at or below 1,000 m/s. Below 6 m, velocity structure becomes laterally discontinuous, putting higher Vp of around 2,000 m/s at shallower depths toward the center of the spread, which rapidly slopes away in either direction down to 60 m depth. Below 60 m and above 130 m both models depict mostly constant Vp of around 3,000 m/s with isolated patches of higher Vp up to 3,500 m/s and as low areas down to 1,200 m/s. Below 130 m depth both models depict a sharp Vp increase up to 4,000 to 5,000 m/s. Outside both spreads, where velocities are less constrained, Vp drops to below 1,000 m/s and are considered less realistic. Where the two Vp models differ is towards the center of each spread. Velocities in the Fall Creek model show laterally variable structure between geophones 60 and 111 from depths of around 20 to 80 m. With depth, velocity fluctuates between 2,000 to 3,500 m/s, resulting in several velocity reversals down to 80 m depth. Laterally, velocities are generally higher to the east. The Pe Ell model shows a distinct velocity low between geophones 84 and 110 at a depth of 50 m, resulting in strong velocity reversal surrounded by higher Vp.

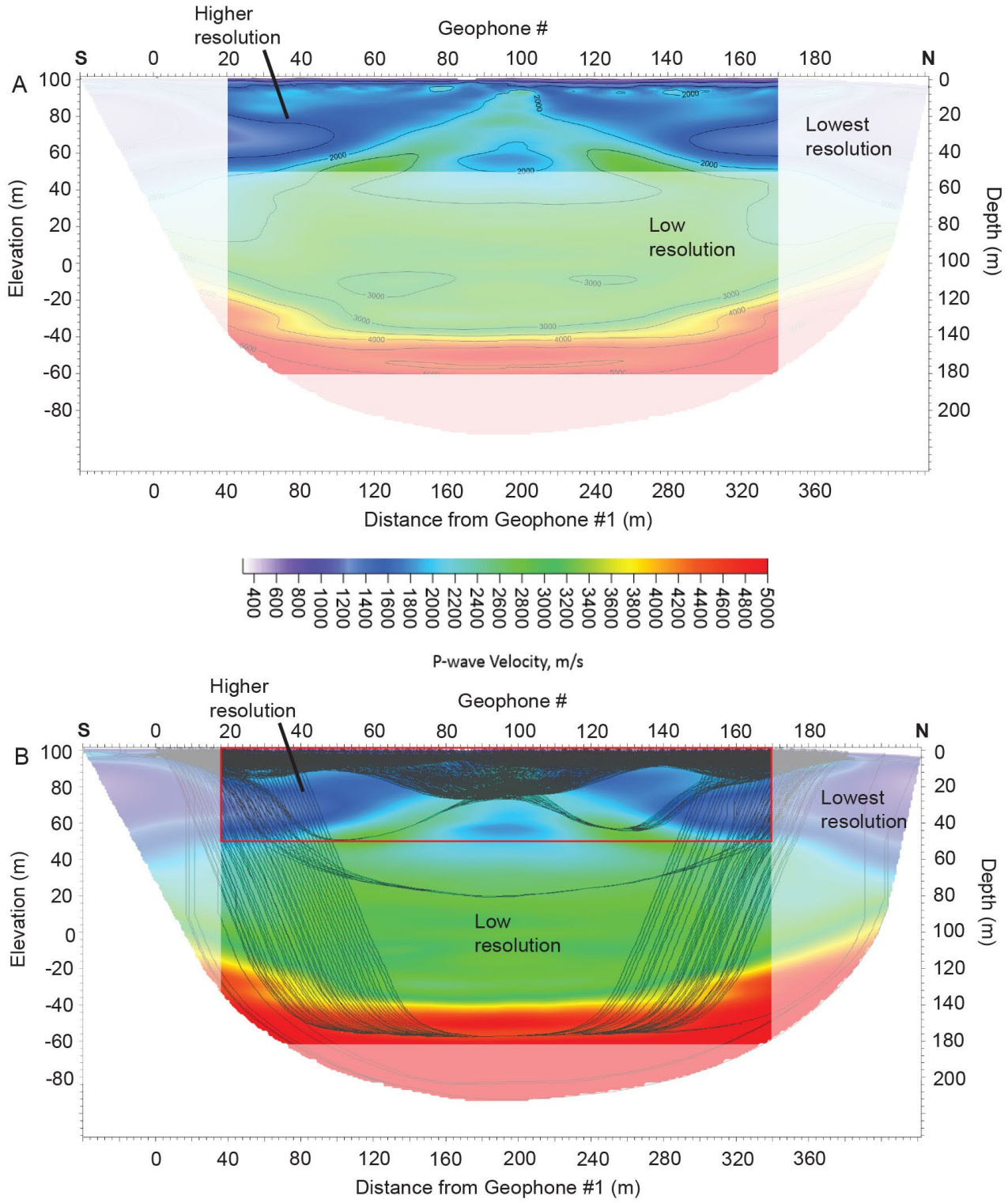

Figure C-2. Velocity and raypath model for site SG-6 near Pe Ell. A) Velocity model. Shaded areas are lower resolution. The lowest has very few rays sampling the velocity structures. The low resolution area has more rays, but few crossing raypaths. The higher resolution area has the most crossing rays; we only use variations within this area to add to our interpretations of the reflection data. B) Raypaths for final iteration of the velocity inversion. Noted areas with different resolution match those in (A).

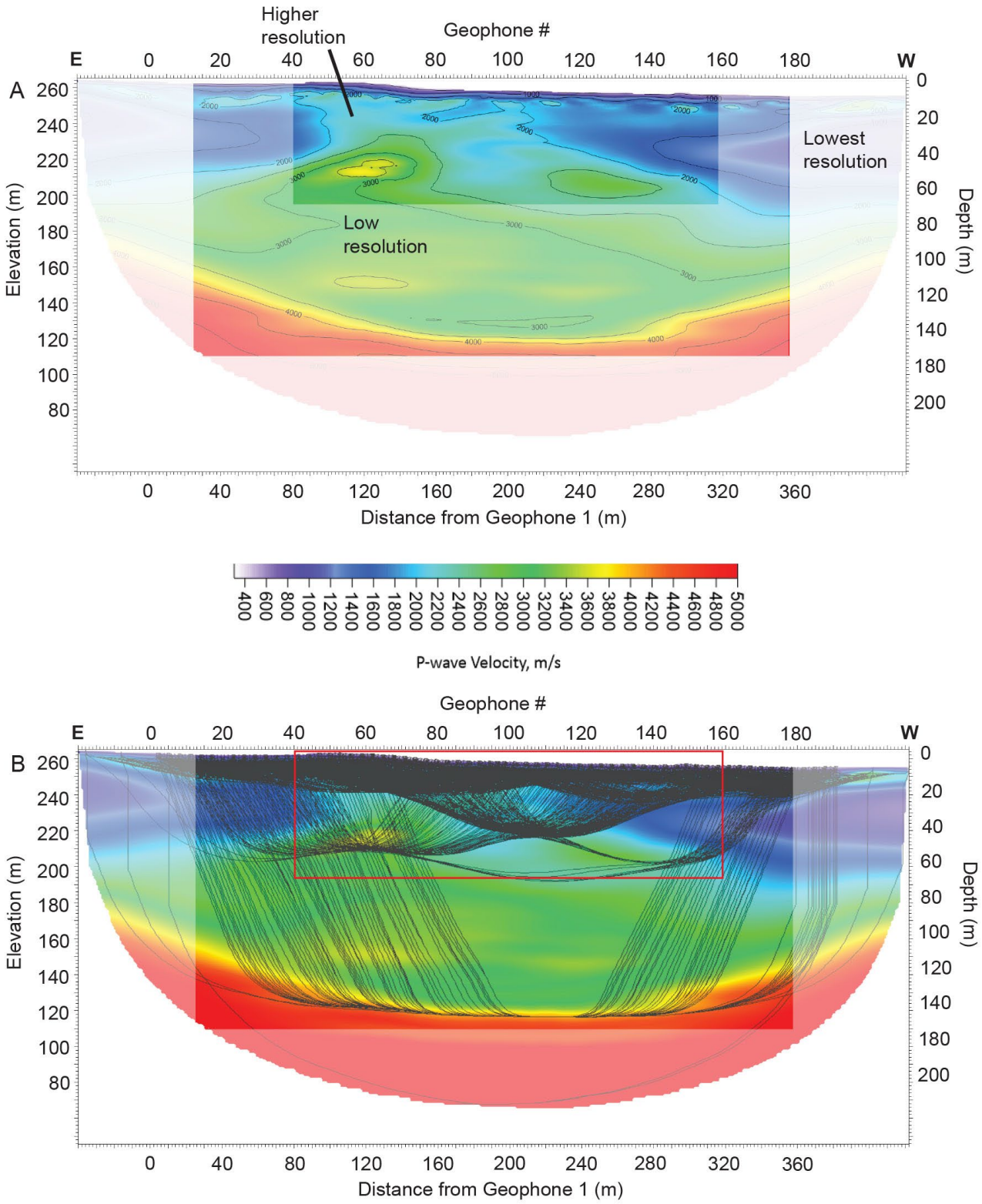

Figure C-3. Velocity and raypath model for site SG-7 at Fall River. Note that models have horizontal axes reversed from reflection images in Figure 6-17. A) Velocity model. Shaded areas are lower resolution. The lowest has very few rays sampling the velocity structures. The low resolution area has more rays, but few crossing raypaths. The higher resolution area has the most crossing rays; we only use variations within this area to add to our interpretations of the reflection data. B) Raypaths for final iteration of the velocity inversion. Noted areas with different resolution match those in (A).

Summary of Major Findings Applied to Research Goals

SG-6 (PE ELL GAP)

We interpret fault-related deformation of Miocene deposits in both the seismic and ER surveys. Neither the ER survey nor the seismic survey provide compelling evidence for Quaternary deformation. However, neither survey are particularly well constrained at the depths needed to assess this (~7 m). Ground-penetrating radar surveys revealed an ambiguous reflector that could be fault related, and is at a depth within the Quaternary sediments, but we were unable to rule out fluvial sedimentary processes as the source of the reflector. Similarities in both the seismic and ER survey allow for confident interpretations at this site. The combined data indicate faulting after the late Miocene (Steely and others, 2021).

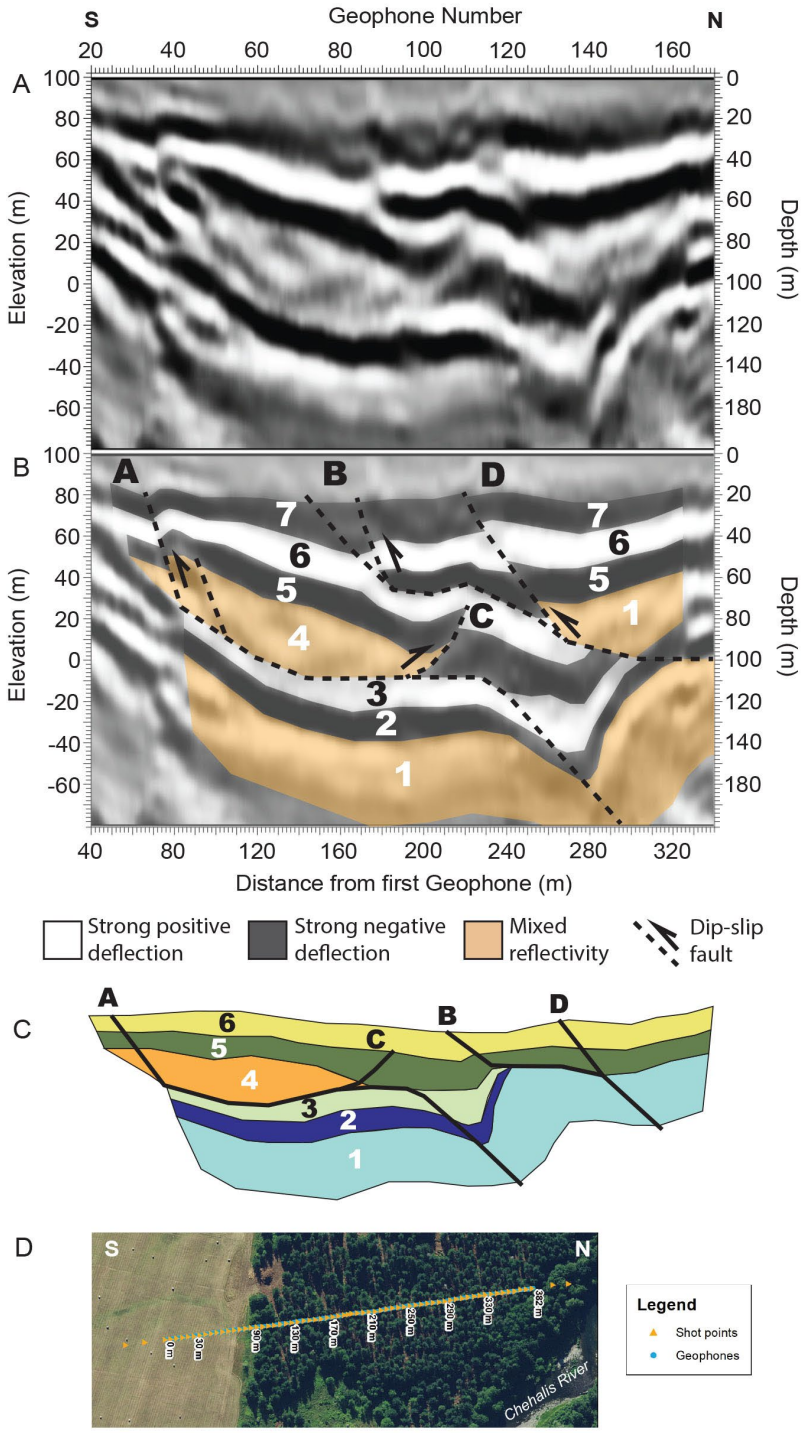

Figure 6-13 (right). Seismic reflection line for site SG-6 at the Pe Ell gap, interpreting a thrust fault system. A) Seismic reflection data. Apparent dips in all reflectors at the north and south ends are due to velocity pull-up effects. B) Interpretation. Letters label faults and numbers label reflectors referenced in the text and in part C. C) Sketch showing reflectors interpreted in part B with appropriate faults and reflectors labeled. It is not strictly balanced, but constructed with structural balancing principles in mind. The reconstruction helps reveal folding and onlapping stratigraphy from this interpretation that would have predated the faulting, perhaps from fault A at a time when it was blind. D) Aerial photo of seismic line location with distance from Geophone #1 labeled.

SG-7 (FALL RIVER)

We interpret fault-related deformation of Eocene to Oligocene Lincoln Creek Formation in both seismic and ER surveys. Evidence for Quaternary deformation within the ER survey is ambiguous. There is no evidence for Quaternary deformation in the seismic survey, although the survey lacks resolution at the depths where Quaternary sediment is most likely (Steely and others, 2021).

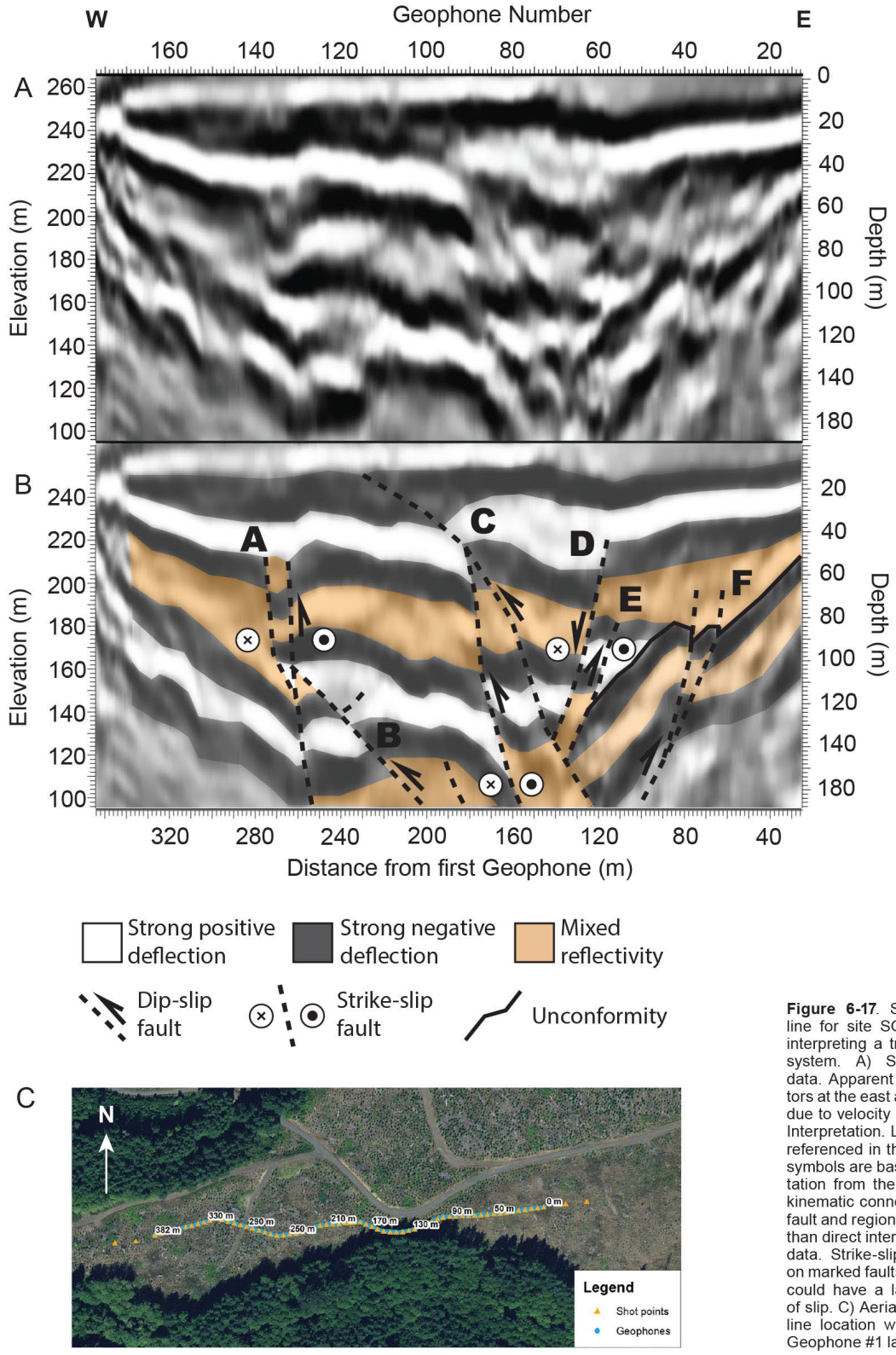

Figure 6-17. Seismic reflection line for site SG-7 at Fall River, interpreting a transpressive fault system. A) Seismic reflection data. Apparent dips in all reflectors at the east and west ends are due to velocity pull-up effects. B) Interpretation. Letters label faults referenced in the text. Transform symbols are based on our expectation from the Fall River fault's kinematic connection to the Doty fault and regional tectonics rather than direct interpretation from the data. Strike-slip motion is likely on marked faults, though all faults could have a lateral component of slip. C) Aerial photo of seismic line location with distance from Geophone #1 labeled.

Steely, A., Anderson, M., von Dassow, W., Reedy, T., Lau, T., Horst, A., Amaral,, C., Cakir, R., West, T., Stanton, K., Linneman, C., Lockett, A., Duckworth, C., Woodring, D., Tepper, J., Staisch, L., 2021, Geologic and Geophysical Assessment of Tectonic Uplift and Fault Activity in the Doty and Willapa Hills, Southwest Washington: Final Report, Washington Geological Survey Report, 279 p.

Telford, W.M., Geldart, L.P., Sheriff, R.E., 1990, Applied Geophysics, 2nd Ed. Cambridge, 770 pp.

Veeken, C. H., van Moerkerken, B., 2013, Seismic Stratigraphy and Depositional Facies Models, EAGE Publications, Houten, The Netherlands.